

An overview of the unique absorption and scattering characteristics of gold nanoparticles: experimental and theoretical study

Hana Abdullah Alluhaybi^{a,b}, Sib Krishna Ghoshal^a and Bahía Othman Alsobhi^b

^aDepartment of Physics, Faculty of Science, Universiti Teknologi Malaysia, 1 Johor Bahru, Malaysia; ^bDepartment of Physics, Faculty of Sciences, Taibah University Almadeenah Almonawarah, Medinah, Saudi Arabia

ABSTRACT

Theoretical prediction of the unusual optical properties shown by the gold (Au) nanomaterials remains challenging. Based on this fact, some colloidal Au nanoparticles (AuNPs) were prepared in ethanol and deionized water using the versatile pulse laser ablation in liquid (PLAL) method and characterized. The pulsed laser irradiation energy-dependent optical absorbance and morphology of these AuNPs were determined. Analytical Mie–Gans scattering model was applied to interpret the experimentally observed absorption spectra of these colloidal AuNPs. In addition, the AuNPs size and shape-dependent absorbance were predicted accurately by fitting the recorded spectra with the analytical model simulation. The results revealed that the dielectric function of the AuNPs played a considerable role to realize the best fit of the experimental absorption data. The average sizes of the AuNPs predicted by the proposed analytical model were tallied well with the experimentally measured ones. It is found that an accuracy of more than 8% on the particle size between experimental and predicted data. It is established that the modified Mie–Gans scattering model can provide a better understanding of the distinct absorption attributes of the colloidal AuNPs synthesized by the PLAL method in various liquid media.

Highlights

- Some AuNPs were prepared in ethanol and deionized water using the PLAL method.
- The morphology and absorbance of the produced AuNPs were determined.
- Absorption and scattering traits of these NPs were explained via the modified Mie–Gans model.
- Proposed AuNPs with distinct optical traits may be beneficial for practical applications.

ARTICLE HISTORY

Received 9 June 2022
Revised 20 September 2023
Accepted 19 January 2024

KEYWORDS

AuNPs; PLAL; absorbance; Mie–Gans model; dielectric function





1. Introduction

In recent times, intensive studies have been conducted to customize the morphology, structures, chemical, optical and physical properties of gold nanoparticles (AuNPs) desired for varied applications [1]. Particularly, the phenomena related to the localized surface plasmon resonance (LSPR) of the AuNPs received renewed interest owing to their usefulness in sundry practical applications including the surface-enhanced Raman scattering (SERS) [2,3], all-optical switches [4], biomedical diagnoses and imaging [5], nanomedicine, therapeutic drugs, and cancer treatment [6]. Repeated research revealed that the LSPR characteristics of the AuNPs can be tuned by controlling their morphology (shape, size, and geometry), compositions, and surface fictionalizations.

Over the years, different theories and models have been utilized to calculate the optical properties of the

AuNPs [7–9] in which the most common one is the Mie theory [10]. Mie scattering (also known as the Mie theory or non-molecular scattering) is essentially an analytical solution of Maxwell's equations wherein the electromagnetic radiation is scattered elastically by the particles having diameters close to or larger than the incident light wavelength. According to this theory, the AuNP-mediated LSPR effect strongly depends on its size and shape. Thus, the LSPR wavelength of the Au nanostructures can be tuned by customizing the sizes and shapes of the AuNPs via the synthesis procedures. To achieve this goal, numerous fabrication methods of the Au nanostructures have been developed [10–12].

To synthesize high-quality Au nanocolloids various novel methods have been developed [12–15]. Generally, the physical, biological and chemical techniques are used to prepare AuNPs and others [16]. Currently, numerous studies have focused on improving

CONTACT Hana Abdullah Alluhaybi  haalluhaibi@gmail.com  Department of Physics, Faculty of Science, Universiti Teknologi Malaysia, 1 Johor Bahru, Johor 81310, Malaysia; Department of Physics, Faculty of Sciences, Taibah University Almadeenah Almonawarah, B.O. Box 1343, Medinah, Saudi Arabia; Sib Krishna Ghoshal  sibkrishna@utm.my  Department of Physics, Faculty of Science, Universiti Teknologi Malaysia, 1 Johor Bahru, Johor 81310, Malaysia

© 2024 The Author(s). Published by Informa UK Limited, trading as Taylor & Francis Group.

This is an Open Access article distributed under the terms of the Creative Commons Attribution-NonCommercial License (<http://creativecommons.org/licenses/by-nc/4.0/>), which permits unrestricted non-commercial use, distribution, and reproduction in any medium, provided the original work is properly cited. The terms on which this article has been published allow the posting of the Accepted Manuscript in a repository by the author(s) or with their consent.

the speed, non-toxicity, safety, cost and environmental friendliness of the nanoparticles produced by these methods. Nonetheless, these techniques have several limitations related to the difficulty in controlling the morphologies of the NPs (sizes and shapes), sustainability, reproducibility, separation of the NPs, and surface functionalization [13]. To overcome these shortcomings, optical methods for synthesizing various types of organic and inorganic NPs emerged as the promising route. The optical techniques are preferred owing to their accuracy in adjusting the processing parameters, eco-friendliness, simplicity, cost-effectiveness, high yield, scalability, tunable morphology, non-requirement of extra chemicals, and the ability to produce contaminant free nanoparticles with desired properties [17]. Due to this reason, we used the pulsed laser ablation in liquid (PLAL) method due to its simplicity and low cost has been used to produce ultrafine colloidal AuNPs with outstanding purity, high stability and unique surface chemistry.

In order to determine the optical absorption property of the AuNPs the ultraviolet–visible (UV-Vis) spectroscopy is used widely. The UV-Vis spectral analyses allow one to estimate the sizes, concentrations, and degree of aggregations of the prepared AuNPs in the colloidal suspension. Mie theory with the proper modification of the metallic NPs size-dependent dielectric constant and physicochemical properties of the growth environments can be used to interpret the measured absorption spectrum of the AuNPs. Many researchers have highlighted the issues involving the predictability and interpretations of the AuNPs size-dependent SPR absorption spectral peak positions [10,12,18].

According to Bohren and Huffman, the theory of Mie scattering provides the best explanations regarding the absorption traits of the noble metal NPs (especially Au and Ag) [11]. Based on Bohren and Huffman's algorithm [11], the detailed computation of the scattering coefficients and cross-sections of the metallic NPs were carried out. Amendola and Meneghetti [18] improved the Bohren and Huffman's algorithm based on the Mie and Gans model to fit the experimentally observed absorption spectra of the AuNPs wherein the mean size of the NPs were accurately predicted by calibrating the damping frequency (Γ) of the LSPR modes [18]. Despite many theoretical efforts, a comprehensive theory and model to explain the experimentally observed optical characteristics of AuNPs have been deficient [18,19]. Most of the existing models and approaches are not accurate and reliable enough to predict the AuNPs morphology dependence of the LSPR peak position wherein the NPs shape and sizes are influenced by various processing parameters, dielectric environments [2], physical/chemical interaction on the NPs surface/interface, presence of charges on the NPs surface, interparticle separation, and aggregations.

One of the most significant factors that affect the theoretical prediction of the plasmonic properties of

AuNP is its dielectric function. The prediction of the plasmonic properties of free-electron metals in general and AuNPs in particular is based on the experimentally measured dielectric function by Johnson and Christy [20] or theoretically calculated one using the Drude model [11]. In fact, the Drude model does not consider the inter-band transitions that are present in the noble metals and their alloys. Consequently, the optical properties of the noble metals predicted using the Drude model reveal appreciable deviation from the experimentally measured ones. Conversely, for the majority of the practical materials, the interpolated experimental results are utilized for different kinds of calculations. Nevertheless, diverse computational algorithms for the evaluations of the optical properties of noble metals require some precise analytical descriptions or expressions of the frequency-dependent dielectric functions ($\epsilon(\omega)$). On top, the analytical representations often provide an in-depth knowledge of various conditions wherein the inherent parameters of the metallic system may be modified by external perturbation or stimulations. A recent study showed that the dielectric function of the nanoscale metallic structures is dominated by their inter- and intra-band effects [2,21]. However, the theoretical explanation regarding the effects of the complex dielectric function of the AuNPs on their optical absorbance and scattering characteristics has been lacking.

In this work, the Mie–Gans (MG) analytical model was modified by implementing the size-dependent complex dielectric function of the AuNPs. The size distribution of the AuNPs was considered to be Gaussian with an appropriate standard deviation. In addition, the inter-band transitions of AuNPs with various sizes were fitted to the experimentally obtained NPs. These colloidal AuNPs were grown in deionized water (DIW) and ethanol media using the pulse laser ablation in liquid (PLAL) method and characterized thoroughly via diverse analytical tools. First, the dependence of the optical absorbance and morphology of these AuNPs on the pulsed laser irradiation energy and solvent types were evaluated. Next, the analytical Mie–Gans scattering model was used to explain the experimentally obtained colloidal AuNPs size-dependent absorption spectra. Matlab program was used to fit the analytical model-simulated AuNPs size and shape-dependent absorption spectra with experimentally recorded ones. The AuNPs morphology and nature of the solvent were found to play a significant role in the dielectric functions and absorption properties of the AuNPs.

2. Experimental

2.1. Synthesis of AuNPs

Figure 1 displays the experimental arrangement of the PLAL technique used to produce the colloidal AuNPs. In this procedure, a pulsed Nd:YAG (neodymium-doped yttrium aluminium garnet; Nd:Y₃Al₅O₁₂) laser

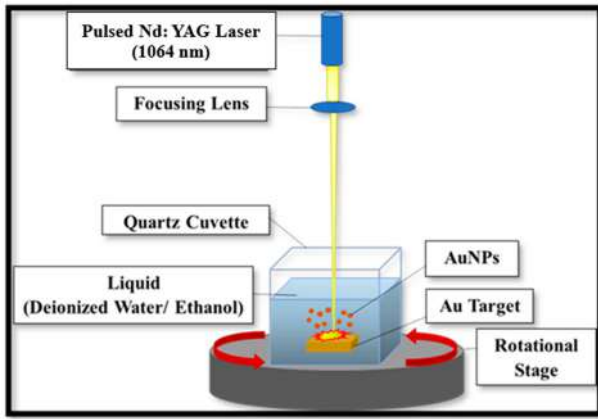


Figure 1. Illustration of the PLAL method setup for AuNPs preparation.

(Q-switch) was used to ablate the Au target immersed in the liquid. The wavelength, pulse duration, and pulse repetition rate of the laser were 1064 nm, 8 ns, and 1 Hz, respectively. The laser pulse irradiation with various ablation energies (96.6, 226, 286, and 318 mJ) was focused (with a spot size of 1.3 mm) on the gold target using a lens of focal length 100 mm. The dimension (length \times breadth \times thickness) of the Au target was (20 mm \times 10 mm \times 2 mm). The gold plate (target) was first rinsed using ethanol followed by DIW to eliminate the contaminants present at the surface. Then, the uncontaminated gold plate was dipped at the bottom surface of a quartz cuvette (volume of 27 cm³) filled with 5 mL of liquid medium (DIW and ethanol). The separation between the rotational stage and pulsed laser source was 70 mm. During the laser ablation process, the cuvette was revolved gradually via a step-motor at a fixed speed to obtain the homogeneous distribution of the generated AuNPs. Such slow rotation of the cuvette was automated to prevent the formation of craters on the surface of the Au target by laser pulse irradiation. The fluences of ablating laser pulse irradiation corresponding to various intermediate laser ablation energies (LAE) of 96.6, 226, 286, and 318 mJ were 7.28, 17.03, 21.55, and 23.96 J/cm². A total of four colloidal AuNPs samples were prepared in each liquid medium (ethanol and DIW).

2.2. Characterizations of AuNPs

The optical absorption spectra of the prepared colloidal AuNPs suspension were measured using the UV-Vis spectroscopy (Perkin-Elmer, Lambda 25) where the samples were placed in the quartz cuvette with a path length of 0.5 cm. The existence and morphology of the colloidal AuNPs were imaged using a transmission electron microscope (TEM, JEOL JEM 2100 set at the working accelerating voltage of 200 kV). All the characterizations of the samples were performed at room temperature.

3. Theoretical formulation

3.1. Modification of the Mie-Gans analytical model

3.1.1. Inclusion of the dielectric function of AuNPs

The interaction of the metallic nanostructures with their surrounding environment is fundamentally significant in determining the optical and transport properties [2,18]. Currently, the determination of the frequency-dependent refractive indices of the noble metallic nanostructures generated wide interest in numerous experimental and theoretical due to their ever-growing applications [8]. The interactions of the incident electromagnetic wave of frequency (ω) and wave vector (k) with the metallic nanostructures can be described by the complex frequency-dependent dielectric function ($\varepsilon(\omega)$) of the medium. The expression for $\varepsilon(\omega)$ of the metallic nanostructures can be written as the following local function:

$$\varepsilon(\omega) = n^2(\omega) = (n'(\omega) + in''(\omega))^2 \quad (1)$$

where i the imaginary number, $n'(\omega)$ and $n''(\omega)$ are the respective real and imaginary components of the frequency-dependent refractive index of the metallic nanostructure. The simple analytical formula for the complex frequency-dependent dielectric function ($\varepsilon_D(\omega)$) of metals can be derived from the Drude-Sommerfeld model. For the perfect metal (bulk), the expression of $\varepsilon(\omega)$ supplemented by the relaxation rate of electrons (γ_{bulk}) can be written as:

$$\varepsilon_D(\omega) = \varepsilon_\infty - \frac{\omega_p^2}{\omega^2 + i\omega\gamma_{\text{bulk}}} \quad (2)$$

where ε_∞ includes the bound electrons' contributions to the polarizability, ω_p is the plasma frequency (bulk) and $\gamma_{\text{bulk}} = \frac{v_F}{l_e}$ (with l_e as the mean free path and v_F as the Fermi velocity of the electrons) and in metal is proportional to the rate of the reciprocal mean free time between the collision of the electrons. For Au the value of $l_e = 42$ nm [22].

Based on the metallic band structures, Rioux et al. (2014) introduced a model to evaluate the influence of the morphology (size and shape) on the complex dielectric function of the nanometals [8]. Using this model, the inter- and intra-band transitions were successfully calculated at two critical points [2,8]. The inclusion of these two critical points in the Drude model enabled the expression of $\varepsilon(\omega)$ taking the form:

$$\varepsilon(\omega) = \varepsilon_\infty - \frac{\omega_p^2}{\omega^2 + i\omega\gamma_{\text{bulk}}} + \varepsilon_{cp1}(\omega) + \varepsilon_{cp2}(\omega) \quad (3)$$

where $\varepsilon_{cp1}(\omega)$ and $\varepsilon_{cp2}(\omega)$ are the frequency-dependent complex dielectric function of the nanometal at the two critical points.

3.1.2. Inclusion of various sizes of AuNPs

The optical absorption spectra of the spherical AuNPs can be obtained using the Mie scattering theory [10], solving Maxwell's equations on the restricted geometries mostly spherical ones [11]. The solution consists of modes (l) of different orders starting from the lowest dipolar ($l = 1$) to quadrupolar ($l = 2$) to higher order multipoles. For the spherical particle of radius R , the relation for the extinction (C_{ext}) and scattering (C_{sca}) efficiency can be written as [22–25]:

$$C_{\text{ext}} = \frac{2}{x^2} \sum_{l=1}^{\infty} (2l+1) \text{Re}(a_l + b_l) \quad (4)$$

and

$$C_{\text{sca}} = \frac{2}{x^2} \sum_{l=1}^{\infty} (2l+1) \{|a_l|^2 + |b_l|^2\} \quad (5)$$

Considering the extinction efficiency as the sum of the absorption (C_{abs}) and scattering ones ($C_{\text{ext}} = C_{\text{sca}} + C_{\text{abs}}$), the expression for C_{abs} can be written as [10,25]:

$$C_{\text{abs}} = \frac{2}{x^2} \sum_{l=1}^{\infty} (2l+1) \{\text{Re}(a_l) - |a_l|^2 + \text{Re}(b_l) - |b_l|^2\} \quad (6)$$

The coefficients a_l and b_l (calculated from the Riccati–Bessel functions ψ and ξ) are given by:

$$a_l = \frac{\psi'_{l-1}(mx)\psi_l(x) - m\psi_l(mx)\psi'_{l-1}(x)}{\psi'_{l-1}(mx)\xi_l(x) - m\psi_l(mx)\xi'_{l-1}(x)} \quad (7)$$

$$b_l = \frac{m\psi'_{l-1}(mx)\psi_l(x) - \psi_l(mx)\psi'_{l-1}(x)}{m\psi'_{l-1}(mx)\xi_l(x) - \psi_l(mx)\xi'_{l-1}(x)} \quad (8)$$

$$\begin{aligned} \psi_l(x) &= \sqrt{\frac{\pi}{2x}} J_{l+\frac{1}{2}}(x), \\ \xi_l(x) &= \sqrt{\frac{\pi}{2x}} \left[J_{l+\frac{1}{2}}(x) + iY_{l+\frac{1}{2}}(x) \right] \end{aligned} \quad (9)$$

where J_l and Y_l are the first and second order Bessel functions, respectively. Here, $x = 2\pi\sqrt{\epsilon}R\lambda^{-1}$, with λ is the wavelength of the incident light beam and ζ is the ratio of the refractive index of the nanoparticle to the medium which is defined as:

$$\zeta = \frac{n_p}{n_m} = \sqrt{\frac{\epsilon(\omega)}{\epsilon_m}} \quad (10)$$

where $\epsilon(\omega) = \epsilon_1(\omega) + i\epsilon_2(\omega)$ and ϵ_m is the dielectric function of the surrounding medium [10,25].

The values of extinction, scattering, and absorption cross-sections can be obtained by multiplying the corresponding equations (4)–(6) with the real area of the spherical particle projected onto the plane perpendicular to the incident radiation wave vector. The physical meaning of the extinction cross-section of the metallic nanoparticles is the total region of the incident radiation that is eliminated (absorbed plus scattered) by these nanoparticles. Likewise, the scattering

cross-section of the metallic nanoparticles is a measure of the total area of the incident radiation that is scattered from the incident light path by the nanoparticles. Conversely, the absorption cross-section of the metallic nanoparticles is a measure of the area of the incident radiation that is engrossed by the nanoparticles [22]. Mie theory can accurately predict the multipolar mode-dependent extinction (absorption and scattering) properties of the spherical nanoparticles [23]. For small spherical nanoparticles with radius ($r \sim 10$ nm) much below the incident light wavelength an additional size-dependent term must be added to the dielectric function ($\epsilon(\omega, r)$) for a better match of the experimentally measured values. In fact, considering the effects of both bulk and nanoscale effects, the size-dependent relaxation frequency ($\gamma(r)$) in terms of bulk metal value (γ_{bulk}) can be written as [26,27]:

$$\gamma(r) = \gamma_{\text{bulk}} + C \frac{V_F}{r} \quad (11)$$

where C is a theoretical parameter. It is worth noting that for the large particles ($r > 20$ nm) the complex dielectric function is independent of their size. However, for the nanoscale particles, the size is considered as an intrinsic factor that strongly influences the values of $\epsilon(\omega)$.

3.1.3. Inclusion of different shapes of AuNPs

Mie theory can be extended to calculate the optical spectra of a collection of randomly orientated non-spherical AuNPs with the aspect ratio of R . According to Gans theory, the extinction coefficient (C_{ext}) of N particles having volume V can be evaluated within the dipole approximation. Using the modified Mie–Gans model, the expression of the scattering and absorption cross-section for the non-spherical nanoparticles can be written as [11,25]:

$$C_{\text{sca}} = \frac{8\pi^3 V^2 \epsilon_m^2}{9\lambda^4} \sum_{i=1}^3 \frac{1}{P_j^2} \frac{(\epsilon_1 - \epsilon_m)^2 + \epsilon_2^2}{\left(\epsilon_1 + \frac{(1-P_j)\epsilon_m}{P_j}\right)^2 + \epsilon_2^2} \quad (12)$$

$$C_{\text{abs}} = \frac{2\pi V \epsilon_m^{3/2}}{3\lambda} \sum_{i=1}^3 \frac{\frac{1}{P_j^2} \epsilon_2^2}{\left(\epsilon_1 + \frac{(1-P_j)\epsilon_m}{P_j}\right)^2 + \epsilon_2^2} \quad (13)$$

where P_j represents the depolarization factors along the major axis (a) and two minor axes (b and c) of the non-spherical particles that can be calculated using:

$$P_a = \left(\frac{1-e^2}{e^2} \right) \left(\frac{1}{2e} \ln \left(\frac{1+e}{1-e} \right) - 1 \right) \quad (14)$$

$$P_b = P_c = \frac{1-P_a}{2} \quad (15)$$

The shape factor (e) of the non-spherical nanoparticles in terms of R can be written as [28,29]:

$$e = \sqrt{1 - \left(\frac{b}{a} \right)^2} = \sqrt{1 - \frac{1}{R^2}} \quad (16)$$

where the volume of the non-spherical particle is $V = 4\pi/3 ab^2$. By assuming the nanoparticle size distribution ($\phi(a/b)$) as Gaussian [30] with the standard deviation of σ , one achieves:

$$\phi(a/b) = \frac{1}{\sigma\sqrt{2\pi}} e^{-\frac{(a/b-1)^2}{2\sigma^2}} \quad (17)$$

where $a/b > 1$ [18,30].

In this work, Equations (1)–(17) were used to interpret the experimentally observed morphology (size and shape)-dependent optical properties of the AuNPs.

4. Results and discussion

4.1. Experimental absorption and morphological properties of AuNPs

Figure 2(a,b) shows the UV-Vis absorption spectra of the colloidal AuNPs prepared in DIW and ethanol at different pulse laser ablation energy (LAE), respectively. In both cases, the SPR absorption peak position and spectral width were found to be sensitive to the LAE (Tables 1 and 2). The peak absorbance (Figure 2(a)) was increased accompanied by a blue shift from 524 to 521 nm with the increase in the LAE from 96.6 to 318 mJ, respectively. These observations were attributed to the strong quantum confinement effect (QCE) of the tiny AuNPs, supporting the results obtained from the TEM image analyses. In fact, the stronger QCE of the tinier AuNPs led to an enhancement in the transition energy requirement from the ground to the excited level, thereby causing a blue shift in the SPR peak absorbance. The peak absorbances of the AuNPs prepared in ethanol (Figure 2(b)) were enhanced accompanied by the blue shifts (from 527 to 523 nm) with the increase in the LAE.

The observed differences in the absorption peak intensities and blue shifts of the studied AuNPs clearly indicated their sensitiveness on the changes in the LAE and nature of the liquid media. It was inferred

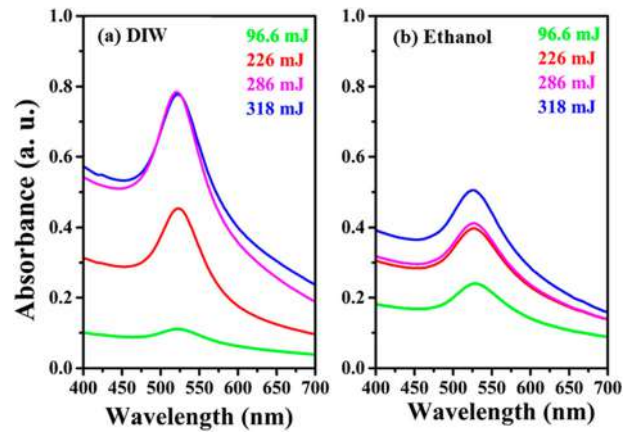


Figure 2. The measured SPR absorbance of the AuNPs produced by PLAL method at different LAE in (a) DIW, (b) ethanol.

that the tinier NPs played the predominant role in the UV-Vis absorption process at room temperature, confirming the strong QCE. These results were supported by the observation made from the TEM image analyses. In addition, the present results suggested that the localized surface plasmon (LSP) modes were critically sensitive to the morphologies (sizes, shapes, geometries and symmetries) of the AuNPs and nature of the liquid growth medium. The LSP resonance (LSPR) occurred when the characteristic LSP frequency of the metal NPs matched with the incident radiation frequency [23]. The LSPR peak absorbance (a measure of the absorption strength of the AuNPs) was indeed determined by the NPs diameter which must be much lower than the incident light wavelength. Clearly, the SPR absorption peak positions and intensities of the proposed AuNPs were determined by their morphologies (shapes and sizes). In short, the overall behaviour in both cases revealed almost the same trend in the absorption parameters, indicating the predominance of the QCE. These findings are comparable with the other state-of-the-art literature reports [14,18]. The colloidal

Table 1. Comparison of the experimental optical absorption properties of the AuNPs grown in DIW at various LAEs with the Mie–Gans model simulation fit using the MATLAB program.

Sample	Measured data fitting by Mie–Gans model					Experimental data			
	LAE (mJ)	Peak position (nm)	D (nm)	σ_G (nm)	FWHM (nm)	Spherical NPs (%)	Peak position (nm)	D (nm)	σ_G (nm)
96.6	522	12.953	0.903	2.125	87	524	30.112	9.421	17.150
226	523	17.893	1.065	2.509	84	523	24.981	11.739	52.428
286	522	16.117	1.333	3.139	67	522	17.516	5.982	8.889
318	521	6.874	1.707	2.608	88	521	7.516	4.007	7.459

Table 2. Comparison of the experimental absorption properties of the AuNPs grown in ethanol at various LAEs with the Mie–Gans model simulation fit using the MATLAB program.

Sample	Measured data fitting by Mie–Gans model					Experimental data			
	LAE (mJ)	Peak position (nm)	D (nm)	σ_G (nm)	FWHM (nm)	Spherical NPs (%)	Peak position (nm)	D (nm)	σ_G (nm)
96.6	527	2.71	1.332	3.136	86	527	3.25	0.369	0.869
226	525	3.76	1.324	3.118	65	526	3.87	1.189	2.801
286	527	3.85	1.227	2.918	66	525	4.75	1.256	2.959
318	524	4.84	1.112	2.618	62	523	4.68	1.944	4.578

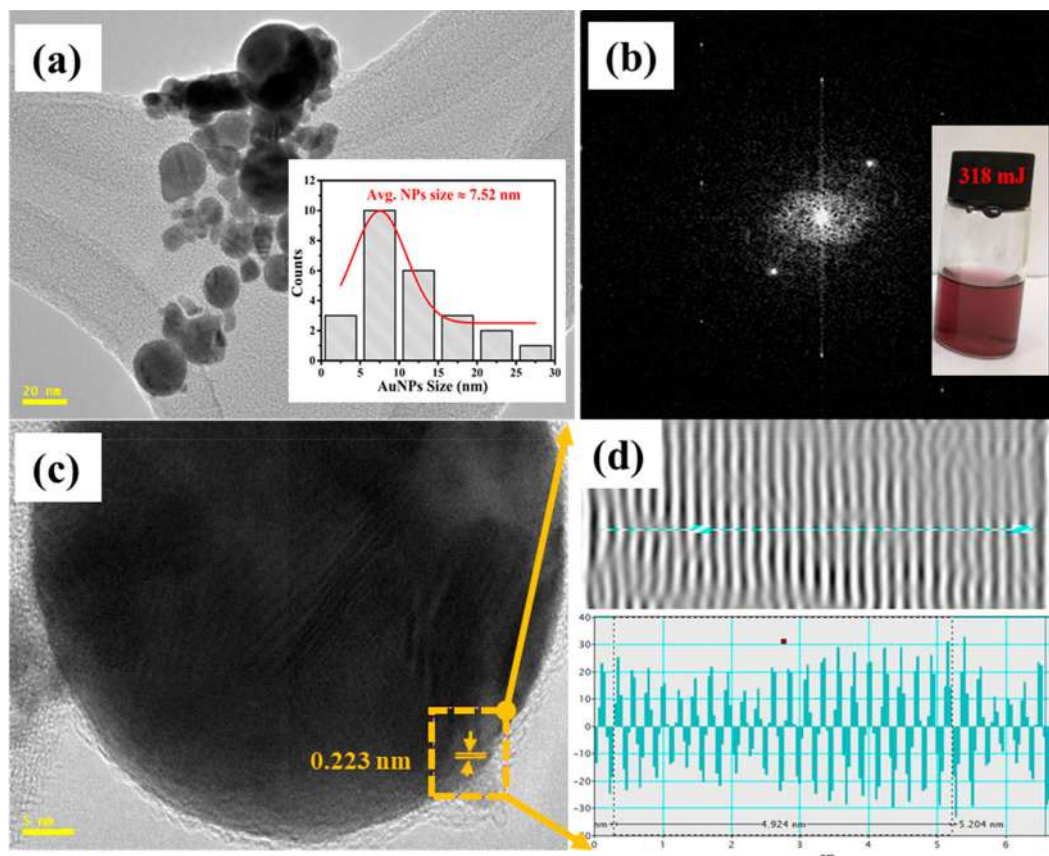


Figure 3. (a) TEM image of colloidal AuNPs produced in DIW at LAE of 318 mJ (Inset: AuNPs size distribution), (b) FFT pattern of the marked part of single AuNP (Inset: colour appearance of the colloidal AuNPs in the bottle), (c) HRTEM image, and (d) SLFP of the selected NP.

AuNPs prepared in both DIW and ethanol at the LAE of 318 mJ revealed the maximum absorbance and were thus selected as the optimum sample for the rest of the analyses.

Figure 3(a) shows the TEM morphology of the optimum colloidal AuNPs synthesized in DIW at LAE of 318 mJ which consisted of spherical NPs with Gaussian size distribution (inset). The average size of the AuNPs was approximately 7.52 nm. Figure 3(b–d) illustrates the single nanoparticle's Fast Fourier transform (FFT) pattern, high-resolution TEM (HRTEM) micrograph, and single lattice fringe profile (SLFP) of the selected portion of the NP (shown as a yellow rectangle). The TEM and HRTEM micrograph confirmed the nucleation of the spherical Au nanocrystallites with well-defined morphologies (sizes and shapes), homogeneities, and narrow size distribution. The lattice spacing of the Au nanocrystalline particles (the yellow rectangle in Figure 3(c)) was found to be 0.223 nm which was also verified by the estimated value of the SLFP (Figure 3(d)).

Figure 4(a) shows the TEM morphology of the optimum colloidal AuNPs synthesized in ethanol at LAE of 318 mJ which consisted of uniformly dispersed high and dense spherical NPs with Gaussian size distribution (inset). The average size of the AuNPs was approximately 4.68 nm which is much smaller than the one grown in DIW, indicating the significant influence of

the growth medium. Figure 4(b–d) illustrates the single nanoparticle's Fast Fourier transform (FFT) pattern, high-resolution TEM (HRTEM) micrograph, and single lattice fringe profile (SLFP) of the selected portion of the NP (shown as a yellow rectangle). The TEM and HRTEM micrographs confirmed the nucleation of the spherical Au nanocrystallites with well-defined morphologies (sizes and shapes), homogeneities, and narrow size distribution. The lattice spacing of the Au nanocrystalline particles (the yellow rectangle in Figure 4(c)) was found to be 0.227 nm which was also verified by the estimated value of the SLFP (Figure 4(d)).

The colloidal AuNPs produced in DIW revealed their aggregation tendency and the formation of elongated structures due to coalescence with the neighbouring NPs. This tendency was mainly due to the broadening in NPs size distribution grown at higher LAE. Nonetheless, this limitation can be surmounted by irradiating the agglomerated colloidal AuNPs suspension to the dispersed laser pulses for a few minutes [31]. In contrast, the colloidal AuNPs prepared in ethanol showed a higher tendency to form smaller nanocrystallites with narrower size distribution. Additionally, the aggregation tendency of the AuNPs produced in DIW was removed by choosing ethanol as growth media. These findings are consistent with the other state-of-the-art literature reports [14,31,32]. Irrespective of the growth medium, the TEM image analyses of the as-prepared

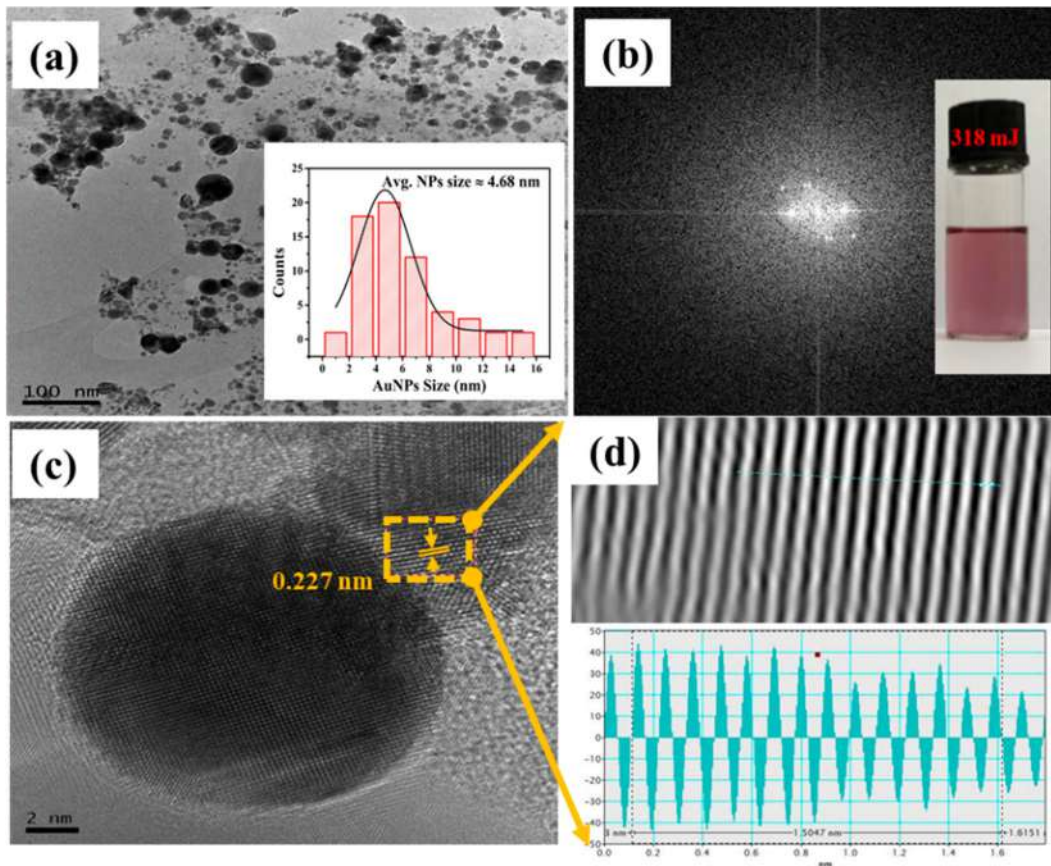


Figure 4. (a) TEM image of colloidal AuNPs produced in ethanol at LAE of 318 mJ (Inset: AuNPs size distribution), (b) FFT pattern of the marked part of single AuNP (Inset: colour appearance of the colloidal AuNPs in the bottle), (c) HRTEM image, and (d) SLFP of the selected NP.

samples clearly showed the nucleation of the tiny spherical AuNPs with well-defined morphologies (shapes and sizes) and homogeneities and narrow size distributions (Gaussian). Briefly, high LAE had a significant effect on the morphology and size distribution of the AuNPs grown in ethanol (Figure 4(a)) than in DIW, displaying a tendency to form smaller NPs with higher density.

With the increase in the LAE, the AuNPs size was reduced and density was improved which was mainly due to the breakdown of the larger AuNPs into tinier NPs. The decrease in the average NPs size can be due to a lower ablation efficiency, wherein the capping effect originated from the organic solvents could hamper the coalescence of the smaller nanocrystallites. In fact, the productivity of the AuNPs in the organic solvent was comparable or even higher than the one obtained with DIW. Therefore, it is likely that solvent molecules were absorbed on the AuNPs surface and acted as the capping agents, thereby preventing the further growth of the NPs. This in turn enabled to attain the thermal equilibrium, thus leading to the development of smaller AuNPs.

4.2. Experimental data fitting using modified Mie-Gans model

The Mie-Gans equations were simulated to fit the experimentally observed extinction spectral profile. The

MATLAB R2015b software (MathWorks) was used as the high-level mathematical programming language to simulate the analytical Mie-Gans model expressions. The codes containing the fitting profile calculation was based on the Equations (4)–(17). The parameter R is replaced by two new important parameters namely the centre of distribution (R_c) and its standard deviation (σF). The values of these parameters were sufficient to define the absorption spectral profile of the colloidal AuNPs suspension prior to the estimation of the particle dimensions and other optical properties. The dielectric function of the AuNPs via a critical point method was implemented into the MATLAB code.

The calculated absorption spectra were improved to allow the shift in the simulated spectra for each data value. This shift enabled to enhancement of the match with the location of the experimental SPR peak intensity (SPR Max). The initialization of the fitting simulation was acquired by estimating the initial average radius (r) by matching the input spectral region around 450–600 nm with the Mie model. Conversely, the initial contribution of the spheroidal shape particles and their distributions were attained by matching the spectral region beyond 600 nm using the Gans model. The validation of the model expression was performed by fitting it to the experimental spectra which were roughly estimated via a root sum of square's analysis (RSS) for every 1 nm wavelength interval (wavelength, x -axis) normalized at

their SPR maximum. Consequently, the present strategy provided an in-depth understanding of the SPR absorption spectra of the colloidal AuNPs with more precise fitting results. It is important to note that all the previous work used the RSS for every 5 nm wavelength interval thus the fit was poor compared to our results [10,18,30]. The nearer the RSS value to one ($RSS \approx 1$), the closer the regression line could approach all the points on the experimental plot. The matching spectra were optimized by varying the average radius with $r = 0.5$ nm ($0.5 < r < 50$ nm), Gaussian size distribution with $\sigma_F = 0.1$ ($1 < \sigma_F < 2.5$), standard deviation of the Gaussian distribution $\sigma_G = 0.2$ ($0.5 < \sigma_G < 2.7$), and fraction of the spheroidal to spherical AuNPs of $f = 1\%$ ($40\% < f < 100\%$). As aforementioned, the Mie model considers the spherical AuNPs and is thus incapable of reproducing the SPR absorption spectra

(for the wavelength more than 520 nm) of the colloidal suspension containing some significant fraction of the non-spherical NPs. Conversely, the Mie-Gans fitting renders a better match even at a wavelength above 520 nm.

Figures 5 and 6 display the Mie-Gans model equations simulated optimum fitting of the experimental absorption spectra of the colloidal AuNPs prepared in DIW and ethanol at the LAE of 318 mJ, respectively. Figure 5(a) shows the fitting of the experimental absorbance (black solid line) of the colloidal AuNPs grown in DIW at LAE of 318 mJ using theoretical Mie-Gans model-simulated absorption spectra (red dotted line). Inset-a illustrates the corresponding size distribution fitted to the normal distribution curve (red line) with the fitting parameters of $R_C = 3.5$ nm, $\sigma_G = 1.7$, spheres = 88%. Clearly, the theoretically

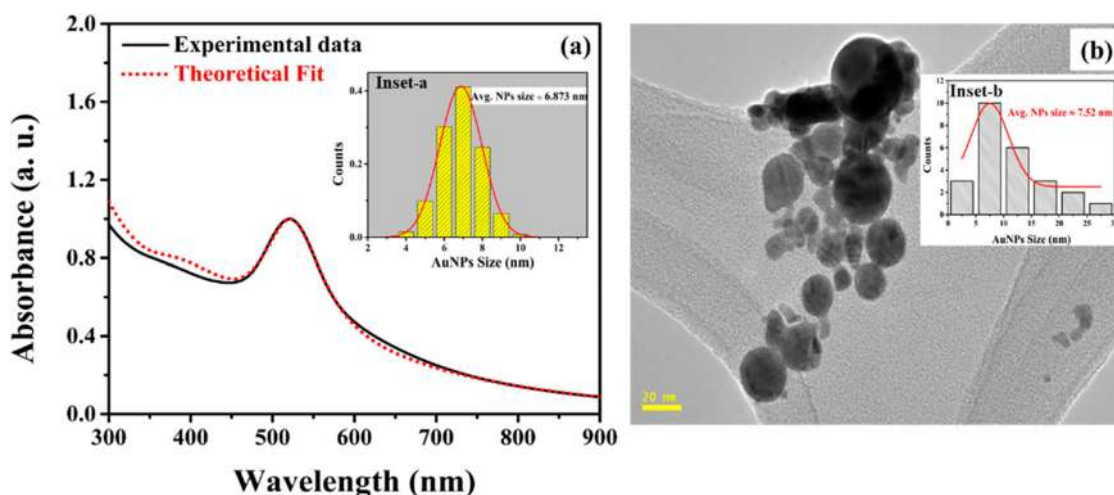


Figure 5. (a) Experimental absorption spectra (black solid line) of the AuNPs grown in DIW at the LAE of 318 mJ fitted with the Mie-Gans model-simulated spectra using MATLAB program (red dotted line) and (b) HRTEM image of the AuNPs. Inset-a and Inset-b are the corresponding size distribution fitted to the normal distribution curve (red line). The fitting parameter for the theoretical model are $R_C = 3.5$ nm, $\sigma_G = 1.7$, spheres = 88%.

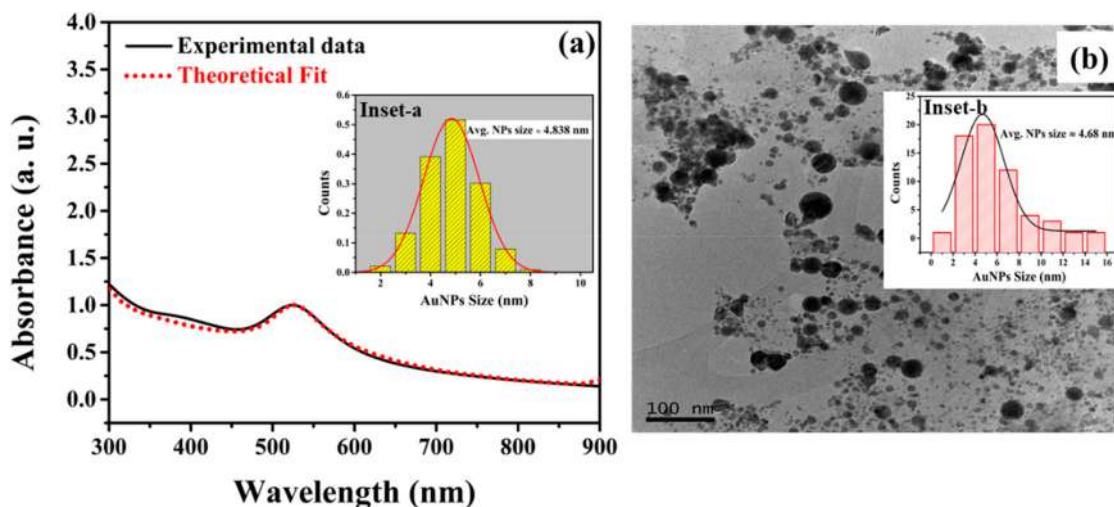


Figure 6. (a) Experimental absorption spectra (black solid line) of the AuNPs grown in ethanol media at the LAE of 318 mJ fitted with the Mie-Gans model-simulated spectra using MATLAB program (red dotted line) and (b) HRTEM image of the AuNPs. Inset-a and Inset-b are the corresponding size distribution fitted to the normal distribution curve. The fitting parameter for the theoretical model are $R_C = 2.5$ nm, $\sigma_G = 1.94$, spheres = 62%.

(from Mie–Gans model) calculated absorption spectra were well-fitted with the measured one, indicating the validity of the proposed Mie–Gans model for interpreting the experimentally observed absorbance of the PLAL-grown colloidal AuNPs. In addition, the obtained slight departure (over estimation) of the model predicted spectral profile in the lower wavelength region (300–450 nm) from the experimentally measured one may be due to the simplicity of the model that needs further improvement. Affandi et al. [30] produced AuNPs in DIW using the PLAL technique and obtained comparable absorbance to the present study. It is further argued that the smaller particles were coalesced together to form larger particles thereby resulting in the highly concentrated tiny AuNPs in the suspension. This disclosure was reconfirmed from the HRTEM images (Figure 5(b)) of the colloidal AuNPs in DIW with the corresponding size distribution (Inset-b) fitted with a normal distribution curve (red solid line). Table 1 compares the experimental optical absorption properties of the AuNPs grown in DIW at various LAEs with the one obtained using the theoretical Mie–Gans model simulation fit.

Figure 6(a) shows the fitting of the experimental absorbance (black solid line) of the colloidal AuNPs grown in ethanol at LAE of 318 mJ using theoretical Mie–Gans model-simulated absorption spectra (red dotted line). The standard deviation and percentage of colloidal non-spherical particles in the liquid media were decided by the preparation method. Yet again, the theoretically calculated absorption spectra were well-matched with the experimentally measured one, confirming the accuracy of the proposed Mie–Gans model for predicting the absorbance of the prepared AuNPs. Furthermore, the observed slight departure (underestimation) of the model-simulated spectra in the lower wavelength region (300–450 nm) from the experimental one might be due to the simplicity of the Mie–Gans model that requires more improvement. Inset-a shows the corresponding size distribution fitted to the normal distribution curve (red line) with the fitting parameters of $R_c = 2.5$ nm, $\sigma_G = 1.94$, spheres = 62%. Present results are in good agreement with the earlier report on the AuNPs prepared in ethanol [18]. The colloidal AuNPs grown in ethanol were much smaller than the one produced in DIW and well dispersed in the liquid medium as verified from the HRTEM images (Figure 6(b)) with the corresponding size distribution (Inset-b) fitted with the normal distribution curve (red solid line). Table 2 compares the experimental optical absorption properties of the colloidal AuNPs grown in ethanol at various LAEs with the one obtained using the theoretical Mie–Gans model simulation fit.

The comparison of the experimental optical absorption properties of the AuNPs grown in DIW and ethanol with various LAEs (Tables 1 and 2) such as the peak position, full width at half maximum (FWHM) and mean crystallite size (D) estimated from the HRTEM with the theoretical Mie–Gans model fit clearly indicated the

validity of the proposed model. The fitting parameters were the average diameter of the AuNPs (D) and its standard deviation (σ_f) of the normal size distribution (Histogram). In addition, the Mie–Gans fitting interval was compared with the HRTEM analysis in terms of the mean diameter D and size distribution (shown in the Inset-a of Figures 5 and 6) It is worth noting that for the first time, we used the dielectric function of the pure AuNPs and improved the theoretical fit remarkably. All other earlier researchers [10,18] used the bulk Au experimentally dataset and consequently, the predicted results using their models revealed some departure from the experimentally observed absorption spectra.

5. Conclusions

This paper evaluated both experimentally and theoretically the absorption and scattering attributes of the colloidal AuNPs prepared in DIW and ethanol at various LAEs using the versatile PLAL technique. Four samples in each liquid medium were synthesized and characterized. The LAE-dependent morphology and absorbance of these AuNPs were determined to make contact with the modified analytical Mie–Gans model. The experimental data on the structural and optical properties such as the NPs size, morphology, absorbance, SPR peak and so on were understood using the proposed theoretical model, where the accuracy of the theoretical prediction depended on the fitting parameters selection. The experimental optical absorption spectra of the obtained optimum colloidal AuNPs (prepared at LAE of 318 mJ) were well-fitted and predicted using the analytical Mie–Gans model. This was achieved by improving the well-established analytical model based on the Mie theory where the critical point dielectric function of the AuNPs instead of the commonly used bulk Au dielectric function (obtained from the experimental data) was incorporated in the model for the first time. This critical point dielectric function was highly sensitive to the alteration in the inter-band and intra-band transitions for the electronic band structure of the AuNPs that was obtained theoretically without acquiring the experimental data. Consequently, we achieved a higher degree of accuracy in the theoretical fit to the experimental absorption spectra of the AuNPs. In addition, the MG model allowed the excellent fitting of the experimental data for the multifunctional pure (with respect to the surrounding environment parameter) tiny colloidal AuNPs produced in DIW and ethanol via the PLAL strategy. On top, the proposed Mie–Gans model could accurately estimate the AuNPs standard deviation and size distribution using the Gaussian distribution, indicating its validity to interpret the experimental SPR absorption properties of the AuNPs. It was demonstrated that the model fitting parameters can be customized easily for other nanoparticles with the characteristic SPR absorption in the UV-Vis like silver, copper, and noble metals alloys.

Disclosure statement

No potential conflict of interest was reported by the author(s).

Funding

The authors are grateful to UTM and Malaysian Ministry of Higher Education for the financial support through grants GUP/RU/UTMFR Vote 20H65 and FRGS/KPT 5F050. Hana is grateful to Taibah University and UTM for continuous financial support and study leave.

References

- [1] Xiao T, Huang J, Wang D, et al. Au and Au-based nanomaterials: synthesis and recent progress in electrochemical sensor applications. *Talanta*. 2020;206:120210. doi:10.1016/j.talanta.2019.120210
- [2] Peña-Rodríguez O. Modelling the dielectric function of Au-Ag alloys. *J Alloys Compd*. 2017;694:857–863. doi:10.1016/j.jallcom.2016.10.086
- [3] Aldosari FMM. Characterization of labeled gold nanoparticles for surface-enhanced Raman scattering. *Molecules*. 2022;27(3):892. doi:10.3390/molecules27030892
- [4] Ghoshal SK, Sahar MR, Rohani MS, et al. Nanophotonics for 21st century. In: *Optoelectronics-devices and applications*. IntechOpen; 2011.
- [5] Falahati M, Attar F, Sharifi M, et al. Gold nanomaterials as key suppliers in biological and chemical sensing, catalysis, and medicine. *Biochim Biophys Acta Gen Subj*. 2020;1864(1):129435. doi:10.1016/j.bbagen.2019.129435
- [6] Taghizadeh S, Alimardani V, Roudbali PL, et al. Gold nanoparticles application in liver cancer. *Photodiagn Photodyn Ther*. 2019;25:389–400. doi:10.1016/j.pdpdt.2019.01.027
- [7] Ghoshal SK, Sahar MR, Dousti MR, et al. Model for up-conversion luminescence in silver nanoparticles embedded erbium-doped tellurite glass. *Indian J Pure Appl Phys*. 2012;50:555–565.
- [8] Rioux D, Vallières S, Besner S, et al. An analytic model for the dielectric function of Au, Ag, and their alloys. *Adv Opt Mater*. 2014;2(2):176–182. doi:10.1002/adom.201300457
- [9] Derkachova A, Kolwas K, Demchenko I. Dielectric function for gold in plasmonics applications: size dependence of plasmon resonance frequencies and damping rates for nanospheres. *Plasmonics*. 2016;11(3):941–951. doi:10.1007/s11468-015-0128-7
- [10] Jain PK, Lee KS, El-Sayed IH, et al. Calculated absorption and scattering properties of gold nanoparticles of different size, shape, and composition: applications in biological imaging and biomedicine. *J Phys Chem B*. 2006;110(14):7238–7248. doi:10.1021/jp057170o
- [11] Bohren CF, Huffman DR. *Absorption and scattering of light by small particles*. Weinheim: John Wiley & Sons; 2008.
- [12] Méndez E, Fagundez P, Sosa P, et al. Experimental evidences support the existence of an aggregation/disaggregation step in the Turkevich synthesis of gold nanoparticles. *Nanotechnology*. 2020;32(4):045603. doi:10.1088/1361-6528/abbfd5
- [13] Ahmed S, Ikram S. Biosynthesis of gold nanoparticles: a green approach. *J Photochem Photobiol B*. 2016;161:141–153. doi:10.1016/j.jphotobiol.2016.04.034
- [14] Zhang J, Claverie J, Chaker M, et al. Colloidal metal nanoparticles prepared by laser ablation and their applications. *ChemPhysChem*. 2017;18(9):986–1006. doi:10.1002/cphc.201601220
- [15] Laban B, Ralević U, Petrović S, et al. Green synthesis and characterization of nontoxic L-methionine capped silver and gold nanoparticles. *J Inorg Biochem*. 2020;204:110958. doi:10.1016/j.jinorgbio.2019.110958
- [16] Alaqad K, Saleh TA. Gold and silver nanoparticles: synthesis methods, characterization routes and applications towards drugs. *J Environ Anal Toxicol*. 2016;6(4):525–2161. doi:10.4172/2161-0525.1000384
- [17] Lee SH, Jung HJ, Lee SJ, et al. Selective synthesis of Au and graphitic carbon-encapsulated Au (Au@ GC) nanoparticles by pulsed laser ablation in solvents: catalytic Au and acid resistant Au@ GC nanoparticles. *Appl Surf Sci*. 2020;506:145006. doi:10.1016/j.apsusc.2019.145006
- [18] Amendola V, Meneghetti M. Size evaluation of gold nanoparticles by UV–vis spectroscopy. *J Phys Chem C*. 2009;113(11):4277–4285. doi:10.1021/jp8082425
- [19] Shabaninezhad M, Ramakrishna G. Theoretical investigation of size, shape, and aspect ratio effect on the LSPR sensitivity of hollow-gold nanoshells. *J Chem Phys*. 2019;150(14):144116. doi:10.1063/1.5090885
- [20] Johnson PB, Christy RW. Optical constants of the noble metals. *Phys Rev B*. 1972;6(12):4370. doi:10.1103/PhysRevB.6.4370
- [21] Alluhaybi HA, Ghoshal SK, Alsobhi BO, et al. Electronic and optical correlation effects in bulk gold: role of spin–orbit coupling. *Comput Condens Matter*. 2019;18:e00360. doi:10.1016/j.cocom.2018.e00360
- [22] Kreibitz U, Vollmer M. *Optical properties of metal clusters*. Vol. 25. Heidelberg: Springer; 2013.
- [23] Amendola V, Pilot R, Frasconi M, et al. Surface plasmon resonance in gold nanoparticles: a review. *J Phys: Condens Matter*. 2017;29(20):203002. doi:10.1088/1361-648X/aa60f3
- [24] Mätzler C. MATLAB functions for Mie scattering and absorption, version 2. *IAP Res Rep*. 2002;8(1):9.
- [25] Olson J, Dominguez-Medina S, Hoggard A, et al. Optical characterization of single plasmonic nanoparticles. *Chem Soc Rev*. 2015;44(1):40–57. doi:10.1039/C4CS00131A
- [26] Qian X, Park HS. The influence of mechanical strain on the optical properties of spherical gold nanoparticles. *J Mech Phys Solids*. 2010;58(3):330–345. doi:10.1016/j.jmps.2009.12.001
- [27] Grady NK, Halas NJ, Nordlander P. Influence of dielectric function properties on the optical response of plasmon resonant metallic nanoparticles. *Chem Phys Lett*. 2004;399(1-3):167–171. doi:10.1016/j.cplett.2004.09.154
- [28] Link S, El-Sayed MA. Spectral properties and relaxation dynamics of surface plasmon electronic oscillations in gold and silver nanodots and nanorods; 1999.
- [29] Link S, El-Sayed MA. Shape and size dependence of radiative, non-radiative and photothermal properties of gold nanocrystals. *Int Rev Phys Chem*. 2000;19(3):409–453. doi:10.1080/01442350050034180
- [30] Affandi MS, Bidin N, Abdullah M, et al. In situ measurement of gold nanoparticle production. *J Nanophotonics*. 2015;9(1):093089. doi:10.1117/1.JNP.9.093089
- [31] Al-Azawi MA, Bidin N. Gold nanoparticles synthesized by laser ablation in deionized water. *Chin J Phys*. 2015;53(4):201–209.
- [32] Amendola V, Meneghetti M. What controls the composition and the structure of nanomaterials generated by laser ablation in liquid solution? *Phys Chem Chem Phys*. 2013;15(9):3027–3046. doi:10.1039/C2CP42895D